HHS Public Access

Author manuscript

Exp Eye Res. Author manuscript; available in PMC 2021 July 01.

Published in final edited form as:

Exp Eye Res. 2020 July ; 196: 108061. doi:10.1016/j.exer.2020.108061.

CXCR5/NRF2 double knockout mice develop retinal degeneration phenotype at early adult age

Hu Huang[*], **Anton Lennikov**

Mason Eye Institute, Department of Ophthalmology, University of Missouri School of Medicine, - Columbia, Missouri, United States of America

Abstract

The objective of this study is to characterize the retinal degeneration (RD) phenotype of CXCR5/NRF2 double knockout (DKO) mice at the early adult age. CXCR5 KO mice and NRF2 KO mice were bred to create CXCR5/NRF2 DKO mice. The assessment of RD features included fundus and optical coherence tomography (OCT) imaging, periodic acid-Schiff (PAS), and immunofluorescence staining of retinal pigment epithelium (RPE)-choroid flatmounts. Stained samples were imaged with fluorescent microscopy, and Western blots were used to monitor protein expression changes. The staining of cleaved caspase-3 and PNA-lectin was performed to assess the presence of photoreceptor cell apoptosis. Quantification and statistical analyses were performed with Image J and Graphpad software. The young adult (2–6 months) DKO mice exhibited increased hypopigmented spots on fundus and sub-RPE abnormalities on OCT as compared to the CXCR5-KO mice, and C57BL6 WT controls. PAS-stained sections demonstrated aberrant RPE/sub-RPE depositions. The DKO mice had increased sub-RPE depositions of IgG and AMD-associated proteins (β-amyloid, Apolipoprotein-E, C5b-9, and αB-crystallin). The protein expression of AMD-associated proteins and microglia marker (TMEM119) were upregulated at the RPE/BM/choroid complex of DKO mice. The adult DKO mice underwent photoreceptor cell apoptosis compared to the single CXCR5 and NRF2 KO and the WT mice at an early adult age. Mechanistically increased expression of CXCL13 and N-cadherin was observed as a sign of

[*]Correspondence: Hu Huang, PhD, Department of Ophthalmology, University of Missouri School of Medicine, Columbia, 1 Hospital Drive, MA102C, Columbia, MO 65212, USA, Phone: 573-882-9899, huangh1@missouri.edu.

Authors' Contributions

The study was conceived and designed by H.H. and A.L.; H.H. and A.L. performed animal breeding and genotyping; H.H. and A.L. performed *in vitro* and *in vivo* experiments and evaluations. The manuscript was written by H.H. and A.L. and critically revised by H.H. Both authors reviewed and accepted the final version of the manuscript.

Availability of data and materials

All data generated and analyzed in the current study are included in this article. Breeding pairs of $CXCR5^{-/-}.NRF2^{-/-}.Rd8^{wt/wt}$ mice can be provided upon reasonable request to the corresponding author.

Ethics approval

All experiments were approved by the Institutional Animal Care and Use Committee of the University of Missouri School of Medicine (protocol number: 9520) and were in accordance with the guidelines of the Association for Research in Vision and Ophthalmology Statement for the use of animals in ophthalmic and vision research.

Competing interests

The authors declare that they have no competing interests.

epithelial-mesenchymal transition. The data suggest that the CXCR5/NRF2-DKO mice develop RD characteristics at an early age and may serve as a valuable animal model of RD.

Keywords

Age-related macular degeneration; Retinal pigment epithelium; Inflammation; CXCR5; Nrf2; Mouse model; Retinal degeneration; β-Amyloid; Complement

Introduction

Age-related macular degeneration (AMD) is a complex disease, as exemplified by its association with various genetic polymorphisms and environmental risk factors and its heterogeneous clinical manifestations and pathological features, including the early hallmarks of aberrant sub-retinal pigment epithelium (RPE), and sub-retinal deposits such as drusen. (Anderson et al., 2002; Curcio, 2018; Hageman et al., 2001; Sarks, 1980) RPE death and photoreceptor degeneration are involved in geographic atrophy (GA) or the “dry” form of AMD (Datta et al., 2017), whereas sub-retinal invasion of choroidal vessels or choroidal neovascularization (CNV) is a feature of the “wet” form of AMD. (Bhutto and Lutty, 2012) These pathological characteristics are the consequence of both genetic variant predispositions and environmental risk factors. Among the cloned and mapped genes that may predispose individuals to AMD are complement factor H (CFH)(Edwards et al., 2005; Haines et al., 2005; Klein et al., 2005), apolipoprotein E (Apo-E) (Klaver et al., 1998), C-X3-C motif chemokine receptor 1 (CX3CR1), (Schaumberg et al., 2014; Tuo et al., 2004) age-related maculopathy susceptibility 2 (ARMS2), and HtrA serine peptidase 1 (HTRA1). (Cho et al., 2009; Edwards et al., 2008) The known environmental risk factors for AMD include cigarette smoke, blue light exposure, advanced age, high-fat diet, and others. Interactions between multiple AMD risk factors may heighten the pathological processes that damage the photoreceptors and RPE, and thereby resulting in the initiation and progression of AMD.

Reliable and reproducible animal models of AMD are essential for deciphering disease etiopathogenesis and developing effective therapies. Despite the absence of a macula in the mouse retina, mice are widely used to create AMD models, primarily because mouse strains can be easily genetically manipulated and are cost-effective for experimental studies. Several mouse strains developed in recent years recapitulate some of the essential characteristics of human AMD, such as RPE pathologies, sub-RPE deposition, and RPE/photoreceptor death, including mice deficient in antioxidant factor genes, such as superoxide dismutase (SOD1), (Imamura et al., 2006) in nuclear factor erythroid 2-related factor 2 (NRF2). (Zhao et al., 2011) in chemokine receptors, such as C-C motif chemokine receptor 2 (Ccr2)(Ambati et al., 2003) and Cx3cr1(Combadiere et al., 2007) genes. Other experimental strains developed for AMD studies include mice immunized with carboxyethylpyrrole protein (CEP)-adducted protein or antibodies, (Hollyfield et al., 2008; Hollyfield et al., 2010) mice with (Apo-E) (Malek et al., 2005) mutations and mice that lack RPE-derived soluble vascular endothelial growth factor (VEGF). (Saint-Geniez et al., 2009)

Recently we characterized the AMD-like phenotypes of aged C-X-C motif chemokine receptor 5 (CXCR5) knockout mice, such as sub-RPE deposits with drusen appearance and RPE degeneration. Which are associated with increased inflammatory marker cyclo-oxygenase-2, and microglia activation markers ionized calcium-binding adaptor molecule 1 (Iba1) and arginase 1 (Arg-1). As well as AMD-associated proteins such as β amyloid, complement 3d (c3d), and αB-crystallin that are deposited at RPE/sub-RPE space, and their protein levels were escalated in the RPE/BM/choroid complex protein extracts of the aged $CXCR5^{-/-}$ mice compared to the same age wild type controls). (Huang et al., 2017) Moreover, the increased Iba1 and β-amyloid are localized in the sub-retina and in sub-RPE, indicative of a potential role in promoting abnormal sub-RPE depositions and AMD pathogenesis. (Lennikov et al., 2019)

A significant challenge to delineating the etiology and pathophysiology of AMD in animal models is that AMD-like features generally develop in advanced-age animals, necessitating a significant amount of lead time for AMD to develop and thus increasing the costs of research. To circumvent this issue, we sought to develop an animal model in which AMD-like features develop at an early age. In this study, we created a CXCR5/NRF2 double knock out (DKO) mice and characterized their AMD-like features at an early age.

Results

Abnormal Fundus and Sub-RPE Deposits in the adult CXCR5/NRF2 double knockout mice

The breeding program of CXCR5/NRF2 DKO ($CXCR5^{-/-}$.$NRF2^{-/-}$.$Crb1\text{-}Rd8^{wt/wt}$) is presented in Fig. 1. Age and sex-matched $CXCR5^{-/-}$.$NRF2^{+/+}$.$Crb1\text{-}Rd8^{wt/wt}$ (CXCR5 KO) and $CXCR5^{+/+}$.$NRF2^{-/-}$.$Crb1\text{-}Rd8^{wt/wt}$ (NRF2 KO) and WT animals were used as controls. In vivo observations were conducted on 4-months old animals.

As expected, the WT animals demonstrated features of a healthy fundus (Fig. 2A), and the CXCR5 KO mice only had a few hypopigmented spots (Fig. 2B). In contrast, numerous hypopigmented spots were visualized in the fundus of CXCR5/NRF2 DKO mice (Fig. 2C). NRF2 KO controls animals demonstrated normal fundus morphology at 4-months of age (Fig 2D). Quantification analysis confirmed the numbers of hypopigmented spots on the fundus were significantly higher in the DKO mice than in the KO mice and in the WT, CXCR5, and NRF2 controls. (Fig. 2I). The fundus observations were further confirmed by OCT imaging, which demonstrated the ten distinct retinal layers from the ganglion cell layer (GCL) to the choroid of the mid-peripheral retina in both KO and WT controls (Fig. 2E-H). Sub-RPE abnormalities and thinner retina were observed in DKO animals (Fig. 2G). Retinal thickness was significantly reduced in DKO mice (Fig. 2J) compared to the controls along with sub-RPE abnormalities (indicated by white arrows) on the OCT images were also significantly higher in the DKO mice than in the KO mice and in the WT controls (Fig. 2K). Interestingly CXCR5-deficient animals both KO and DKO demonstrated enlarged choroidal vasculature (indicated by yellow arrows) that were not observed in WT or NRF2 KO animals.

Increased Sub-RPE Deposits in the Adult DKO Mice

Periodic acid-Schiff (PAS) staining of eye sections of WT controls, 2 and 4 months old DKO mice, CXCR5 KO, and NRF2 KO mice. WT animals sections demonstrated typical healthy eye morphology (Fig. 3A), where PAS-positive aberrant deposits (indicated by white arrows) were observed in the RPE and sub-RPE in both 2- and 4-m.o. m.o.month-old DKO animals (Fig. 3B-C), but very few in the CXCR5 KO (Fig 3D) and NRF2 KO (Fig 3E) mice. The morphologies of the deposits in DKO mice (punctate and hemispheres) were consistent in shape and location with the hypopigmented spots and sub-RPE abnormalities visualized by fundus examination and OCT images (Fig 2G). Quantifications revealed that the numbers of RPE and subRPE deposits were significantly higher in the DKO mice (both 2 and 4 m.o.) than in the KO mice and WT controls (Fig. 3E).

Increased autofluorescence and endogenous IgG accumulation in the DKO mice

The retinal sections from C57BL6 WT (2 m.o.), DKO (2 and 4 m.o.), CXCR5 KO (4 m.o.) and NRF2 KO (4 m.o.) mice were examined for autofluorescence at the 488nm wavelength (Fig. 4A) and endogenous IgG deposits (Fig. 4B) at the interface of the photoreceptor outer segment (POS), RPE, BM, and choroid. Strong spontaneous fluorescence signals were detected on the POS, RPE, BM, and sub-RPE of the DKO mice at 2 m.o. and progressed to involve the retina at 4 m.o., indicative of an increased lipofuscin A2E depositions. The IgG signals were consistent with the progression of autofluorescence with an increase in DKO 2 m.o. with prominent signals visualizing the RPE layer and retina in DKO 4 m.o. WB results (Fig. 4C-D) demonstrated the progression of IgG signals in DKO mice from 2 m.o to 4 m.o. Interestingly the WB data have indicated an accumulation of predominantly LC IgG in the retina of 4 m.o. DKO mice (Fig 4D) consistent with IgG fluorescent observations (Fig 4B). Quantitative analysis of the WB results indicated a significant increase if the IgG signals of both heavy and light chain IgG in the RPE/Choroid/Scleral complexes and the retinas of the DKO mice (Fig 4E-H).

Increased AMD-Associated Protein Depositions and reduced ZO-1 in the adult DKO Mice

Immunofluorescence (IF) staining of RCSC flat mounts in 6 m.o. mice were conducted to examine the RPE/sub-RPE deposition of the four AMD/drusen-associated proteins — β-amyloid (Aβ; Fig 5A); αB-crystallin (Fig. 5B), apolipoprotein-E (Apo-E; Fig. 5C), complement C5b-9; (Fig. 5D) and ZO-1 (Fig. 5E). The results indicated increased immune reactivity of Aβ and αB-crystallin at the RPE and the sub-RPE space of 6-m.o. DKO mice, but was minimal in CXCR5 and NRF2 KO samples. WT controls produced no signals for AMD-associated proteins. The Z-stack analysis placed the signals to be originated predominantly in the sub-RPE layer. These results were further confirmed with the age progression in histological sections indicating RPE/Sub-RPE localization of the signals as well as the age progression of signal intensity in DKO animals from 2–6 months of age. (Supp. Fig 1, 2)

Barrier function protein ZO-1 was markedly downregulated in RPE/Choroid of 6-m.o. DKO mice, with staining demonstrating patches of the decreased signal along with the abnormal shape of RPE cells. WT, CXCR5 KO, or NRF2 KO at 6-m.o. of age demonstrated the normal distribution of the ZO-1 in the cell to cell interaction sites of the RPE cells.

Immunofluorescence results were further confirmed by the western blot analysis (Fig. 6). Consistent with the whole mount results (Fig. 5E) the ZO-1 protein levels were reduced in the adult DKO mice (4 and 6 months old) compared to the KO mice and the WT controls (Fig. 6A and C). Western blot results further revealed the protein levels of β-Amyloid and were upregulated in 4-month-old DKO mice and further increased in the 6-month-old DKO mice (Fig. 6B and D) as compared with the levels in KO mice and the WT mice (Fig. 6B and F). Apo-E were upregulated at 6-month-old DKO mice, but not at 2 or 4 months old, when compared with the WT and the KO mice (Fig. 6A and E)—aligning with histological sections immunostaining (Supp. Fig 1, 2) and the RCSC whole-mount data (Fig 5A, C) indicating the progression of signals with age. Furthermore, WB analysis has further revealed the increased microglia marker TMEM119 in RCSC lysates (Fig 5A and EC) suggestive of microglia migration towards the RPE layer. These results are consistent with our previously reported observations in aged-CXCR5 KO animals (Lennikov et al., 2019)

Increased photoreceptor apoptosis in the adult DKO Mice

We investigated whether increased photoreceptor apoptotic cell death was present in the adult DKO mice. The retinal flat mounts from the 6-month-old DKO mice and the age-matched WT and KO mice were stained with peanut agglutinin lectin (Fig 7A) and cleaved caspase 3 (Fig 7B). PNA lectin (+) photoreceptors were decreased in the DKO mice compared with the levels in KO and WT mice. Concomitantly, the cleaved caspase 3 (+) cells in the photoreceptor cell layer were markedly increased in the DKO mice compared to the apoptotic cell numbers in retinal specimens from KO mice and WT controls (Fig. 7C). Further quantification revealed that the photoreceptor cell densities were significantly lower in the DKO mice than in the KO mice and the WT controls (Fig. 7C). The numbers of cleaved caspase 3 (+) apoptotic photoreceptor cells were significantly higher in the DKO mice than in the KO and WT mice (Fig. 7D). Interestingly while a small but significantly higher number of apoptotic cells were observed in CXCR5 KO retinas, NRF2 KO mice did not indicate a significant decrease of increase in apoptotic cell numbers (Fig 7D).

Increased expression of CXCL13 and Epithelial-Mesenchymal Transition (EMT) marker N-cadherin in the adult DKO Mice

Primary WT RPE cells can express CXCR5-CXCL13 axis proteins (Sup. Fig 3). IF staining of CXCL13 (Fig. 8A) in RCSC flat mounts, of 6 m.o. adult WT and NRF2 KO mice produced noise levels of CXCL13. However, an increase of CXCL13 in RPE cells in CXCR5 KO and a dramatic increase in the DKO RPE cell layer was observed. Similarly, the presence of EMT marker N-cadherin prominently detected in DKO animals and, to a lesser extent, in CXCR5 KO.

Discussion

Among the perturbed biological pathways and processes in AMD are complement pathways, cytokines, chemokines, phagocytosis, autophagy, lipid metabolism, and oxidative stress, many of which have been investigated to generate animal models of AMD that mimic certain features of AMD observed in humans. AMD-like pathologies in these models are often developing at the advanced age, (Ambati et al., 2003; Rakoczy et al., 2002), and in

some cases, require additional stimuli, such as high-fat diet, exposure to cigarette smoke, blue light (Cousins et al., 2002) or injection by lipid oxidants. (Baba et al., 2010; Hollyfield et al., 2008) To overcome this issue, we sought to generate a mouse model of RD by crossing CXCR5 KO mice and NRF2 KO mice and found that these DKO mice develop the RD phenotypic features at earlier ages.

It is well documented in the literature that NRF2 is a protective transcription factor controlling the gene expression of a wide range of cellular oxidative defense mechanisms. (Bellezza, 2018) $NRF2^{-/-}$ mice demonstrate typical AMD-like characteristics at 12 months and older due to increased oxidative stress (Zhao et al., 2011). The role of NRF2 has recently been implicated in human AMD and prospected as the therapeutic target. (Bellezza, 2018) In our study, NRF2-deficiency on its own did not cause significant changes in the retina up to 6 months of age, which is consistent with literature reports describing the RD phenotype to become prominent by 12 months. (Zhao et al., 2011). Increased oxidative stress, such as induced by nicotine, is implicated in EMT (Chang and Singh, 2019), and smoking is one of the prominent risk factors in AMD. (Velilla et al., 2013) Indeed NRF2 KO mice are reported to be highly susceptible to the cigarette smoke induced lung damage. (Iizuka et al., 2005)

Recently we described retinal degenerative phenotypes in aged $CXCR5^{-/-}$ mice in association with loss of blood-retinal barrier function, microglia cell migration to RPE layer, the accumulation of AMD-associated proteins and the occurrence of specific autoimmune responses as possible driving forces of retinal degeneration. (Lennikov et al., 2019). CXCR5-deficient mice demonstrated substantial sub-RPE accumulation of IgG (Huang et al., 2017), which was later identified as autoantibodies to the AMD-associated proteins, such as annexin-A2, αB-crystallin, ubiquitin-B, and aquaporin-5. CXCR5 might also be necessary for the stabilization of microglial cells and the regulation of their activation state in response to microenvironment changes. We also reported the increase of CXCL13 in RCSC the aged CXCR5-deficient animals but was not entirely clear at the time of the specific cellular source of this protein. (Lennikov et al., 2019) RPE cells can express CXCR5-CXCL13 axis proteins. Our recent work in primary RPE cell cultures derived from CXCR5 KO mice has identified the CXCR5 signaling to be required for the hemostatic functions of RPE cells With CXCR5-deficiency to induce aberrant PI3K-AKT-FOXO1 signaling, impaired autophagy and EMT in vitro (manuscript under review). Interestingly in cancer cells a direct connection between NRF2 and P62 through the physical interaction of the autophagy adaptor p62 with the Nrf2 inhibitor Keap1. (Bartolini et al., 2018) Although exact consequences of these pathways in double CXCR5/NRF2 knockout in the eye cells are still remain to be elucidated. These reports are also consistent with findings of the CXCR5-CXCL13 axis role in EMT in breast cancer cells (Biswas et al., 2014), with upregulated CXCL13 as the main actor. Indeed, a marked increase in CXCL13 within RPE cells layer observed in RCSC flatmounts of DKO mice. Our theory is that increased oxidative stress induced by deficiency of NRF2 exacerbates the homeostatic dysregulation of RPE cells caused by CXCR5 deficiency inducing rapid EMT and subsequently photoreceptor cell loss. The combined CXCR5/NRF2 deficiency demonstrates increased EMT transformation marker N-cadherin in RPE cells. Photoreceptor apoptosis leads to AMD-associated proteins accumulation and deposition. With animal immune system maturation, specific autoimmune

response develops due to loss of blood-retinal barrier function. This is supported by findings of Aβ, AlphaB-crystallin, and APOE in the sub-RPE space of DKO animals with clear age progression. Increased autofluorescence and IgG accumulation supportive of the specific autoimmune response due to impaired BRB in DKO mice. Photoreceptor apoptosis process in the RPE/photoreceptor layers lead to activation of the microglia cells that are migrating towards afflicted photoreceptors and RPE cell layer. This is confirmed by the increased TMEM119 marker in RCSC. We believe a similar process occurs at a much slower rate in CXCR5 KO mice with age becoming prominent after 12–14 months of life. The AMD-like features detected in the aged CXCR5 KO, aged NRF2 KO, and adult DKO mice are summarized in Table 1.

It is worth noting that we carefully bred out the *Crb1-RD8* mutation from both founder breeding lines. While animals on C57BL/6j background usually do not have *rd8* mutation of the *Crb1* gene, it is a common occurrence in animals on C57BL/6N background such as $NRF2^{-/-}$ mice. As recently addressed by Mattapallil et al. the *crb1-rd8* mutation is an emerging problem of retinal degeneration research in mice (Mattapallil et al., 2012).

Statement of limitations:

1. We observed changes in retinal thickness, the number of AMD-associated proteins, and increased cleaved-Caspase 3 positive cells in the retina. However, further functional studies such as electroretinography (ERG) or behavioral studies required to address retinal and visual function at different ages of DKO animals.
2. The exact mechanism of the combined effect of CXCR5/NRF2 deficiency leading to RD in different cell types of retina, RPE, and choroid remain to be elucidated. Several potential mechanisms besides general oxidative stress overload may be involved, such as deficient autophagy, EMT in RPE cells, BRB-dysfunction, loss of retinal immune privileges, specific autoimmune inflammation in the RPE, and the retina.
3. NRF2 KO animals are on the C57BL6/N, where CXCR5 KO animals on predominantly C57BL6/Jwith a small component of the C57BL6/N background. Resulting DKO animals have the complex C57BL6/N/J background that may have unknown effects contributing to the observed phenotypes, that requires further analysis utilizing the genome sequencing and comparison with N and J references genomes.

These new DKO mice may provide to be suitable for the understanding of the underlying mechanisms of RD pathology and the evaluation of new treatment strategies and drug candidates. However, further studies are required to clarify the mechanistic aspects of the interplay between the NRF2 and CXCR5 combined deficiency in the eye and how relevant RD observed in the current study to the human AMD.

Materials and methods

Animals, Genotyping and Breeding Strategy

All experiments were approved by the University of Missouri Institutional Animal Care and Use Committee (protocol number: 9520) and performed in accordance with the "Statement for the Use of Animals in Ophthalmic and Vision Research" of the Association for Research in Vision and Ophthalmology. The [B6.129S2(Cg)-CXCR5tm1$^{Lipp/J}$] (CXCR5 KO), B6.129X1-Nfe2l2^{tm1Ywk}/J (NRF2 KO) and [C57BL/6J] (WT) mice strains were purchased from Jackson Laboratory. CXCR5 mice (https://www.jax.org/strain/006659) and NRF2 mice (https://www.jax.org/strain/017009) are on a mixed C57/BL6J/N background with the predominance of C57/BL6J genome. All mice were housed at the specific pathogen-free animal facilities of the Bone Life Sciences Center at the University of Missouri and were fed normal chow diets and provided with water *ad libitum*.

Genotyping was performed with the assistance of Transnetyx (Cordova, TN, USA), Outsourced PCR Genotyping Services (www.transnetyx.com) by real-time polymerase chain reaction (PCR) genotypic assay. Genomic DNA (50 ng) was extracted from tail tips and amplified using custom-designed genotyping primers (TransnetYX). Animals were validated for knockout of the CXCR5, NRF2 gene, the presence of the neomycin resistance, and LacZ genes, respectively. All mice were screened for the presence of Rd8-associated nucleotide deletion, using the Rd8 genotyping probe designed by Transnetyx, based on our previous Sanger sequencing data of the region 3600–3700 of the Crb1 gene (canonical transcript M_133239). (Lennikov et al., 2019)

The two founder mice were bred to generate CXCR5/NRF2 DKO mice. The RD8 mutation in the Crb1 gene incorporated in the NRF2$^{-/-}$ founder animal, was bred out to achieve the stable CXCR5/NRF2 (DKO) mouse line with wild-type RD8 genotype (CXCR5$^{-/-}$.NRF2$^{-/-}$.Crb1-Rd8$^{wt/wt}$). CXCR5$^{+/+}$.NRF2$^{-/-}$.Crb1-Rd8$^{wt/wt}$ controls were generated by breeding the male CXCR5$^{+/+}$.NRF2$^{-/-}$.Crb1-Rd8$^{mut/wt}$ with C57/BL6 WT female mouse and inbreeding the progeny. The CXCR5/NRF2 DKO, CXCR5 KO, and NRF2 KO mice were maintained and inbreed-crossed to give birth to more progenies for further research. As NRF2$^{-/-}$ animals were heterozygote to Crb1-Rd8 mutation mut/wt, the control NRF2$^{-/-}$ animals CXCR5$^{+/+}$.NRF2$^{-/-}$.Crb1-Rd8$^{wtt/wt}$ were produced by crossing the NRF2-deficient founder animals with C57BL6/J control animals and inbreeding the progeny.

Anesthesia and Euthanasia

During *in vivo* experiments, mice were anesthetized by intraperitoneal injection of ketamine hydrochloride (100 mg/kg body weight) and xylazine (4 mg/kg body weight) at the experimental endpoints of 2, 4 and 6 months of age. For tissue collection, mice were euthanized by intraperitoneal injection of ketamine hydrochloride (300 mg/kg body weight).

Fundus Examination and Optical Coherency Tomography

Mice were anesthetized. Pupils were dilated with 1% tropicamide (Sandoz, US). The cornea was protected with (hypromellose ophthalmic demulcent solution) Gonak 2.5% (Akorn

LLC, Akorn, OH, USA) transparent gonioscopy gel. Fundus examination and optical coherence tomography (OCT) was performed with a Micron IV retinal imaging microscope system (Phoenix Research Labs, Inc., Pleasanton, CA, USA). Fundus hypopigmented spots and OCT abnormalities were quantified by "masked" observer.

Confocal Microscope Imaging

Visible light images were acquired using the EVOS FL Color microscope (Thermo Fisher Scientific, Waltham, MA, USA). Fluorescent z-stack images were acquired with a LeicaSP8 laser confocal microscope (Leica AG, Wetzlar, Germany) max intensity projection was used in representative figures. The resulting stacks orthogonal projections were generated using Image J (NIH, Bethesda, Maryland) from the stack image sequences.

PAS staining, autofluorescence, and immunofluorescent Analysis

The eyeballs were fixed with HistoChoice Molecular Biology fixative (H120–4L, VWR Life Science, Radnor, PA, USA) for 12 hours and stored in phosphate-buffered saline (PBS; 10010023, Thermo Fisher Scientific) until specimens were processed for paraffin embedding and sectioning (5 μm thick) and stained by periodic acid and Schiff reagents staining, as reported previously. (Lennikov et al., 2019) Sections intended for autofluorescence evaluation were deparaffinized, rehydrated, and mounted without staining. The gains were set to minimal autofluorescence in the WT sample. Sections for the detection of autoantibodies accumulation were blocked and permeabilized with 0.5% Triton X-100 (85111, Thermo Fisher Scientific) and blocked with 2.5% bovine serum albumin solution (BSA; A7906–50G, Sigma-Aldrich, St. Louis, MO, USA) for 1 hour at room temperature and incubated overnight at 4°C with antimouse (ab6563) secondary antibody.

The primary antibody used for immunofluorescent analysis in rehydrated sections presented in Table 2. Following PBS-Tween 20 0.05% (PBS-T) washing. The immune reactive signals were visualized by Cy5 conjugated anti-rabbit (ab97077, Abcam), anti-mouse (ab6563, Abcam) and anti-goat (ab150131, Abcam) secondary antibody 1:1,000 (Abcam). Sections were counterstained with 4′, 6-diamidino-2-phenylindole (DAPI) 1:5,000 (Sigma-Aldrich) and mounted with ProLong Diamond antifade reagent (P36961, Thermo Fisher Scientific).

Retina and RPE–Choroid-Sclera Complex Flat Mounts

Mouse retinas were fixed and isolated, as reported previously. (Lennikov et al., 2019) Briefly, under a dissection microscope, the anterior segment tissues and vitreous were removed to produce an eyecup. Then retina was gently separated from RPE–choroid sclera complex (RCSC), and four relaxing radial incisions were made to RCSC and retina in order to produce the flat-mount. The retinas and RCSC were blocked and permeabilized with a solution composed of 2.5% bovine serum albumin (BSA; A9467–100G, MilliporeSigma, Burlington, MA, USA) in PBS overnight with 0.01% Triton-X; RCSC samples were then incubated with primary antibody (Table 2). Retina samples were incubated for 24 hours at 4°C with gentle agitation, in peanut agglutinin (PNA) lectin (1:50, L32460; Thermo Fisher Scientific, Waltham, MA) and cleaved-caspase 3 (Table 2); before being washed three times for 10 min with PBS-T; and mounted with ProLong Diamond antifade reagent (Thermo Fisher Scientific, Waltham, MA, USA). Remaining samples were incubated for 24 hours

with Cy5-conjugated rabbit (ab97077), mouse (ab6563) goat (ab150131) secondary antibody (1:1,000; Abcam, Cambridge, MA, USA) and counterstained with 4′, 6-diamidino-2-phenylindole (DAPI) 1:5,000 (MilliporeSigma, Burlington, MA, USA). After another PBS-T washing, the samples were mounted on slides with ProLong Diamond antifade reagent. Samples incubated with a blocking buffer (primary antibody was omitted), followed by secondary antibody incubation, were used as the background control. The number of PAS-positive cells and cleaved-caspase 3 positive cells in the retina flat mounts were quantified in retinas obtained from 4 mice by the "masked" observer in 5 randomly selected 100 μm^2 areas and averaged.

Western Blot Analysis

Retina and RCSC were isolated on ice, and lysates were prepared as previously described. (Lennikov et al., 2019) Thirty micrograms of total proteins were separated by SDS-PAGE gel (Mini-Protean Precast Acrylamide Gels, Bio-Rad, Hercules, CA, USA) and further transferred to the nitrocellulose membrane (Trans-Blot Turbo transfer pack, Bio-Rad). Membranes were blocked with 2.5% BSA (A9467–100G, MilliporeSigma, Burlington, MA, USA) and incubated with primary antibodies (Table 2). The target protein bands were detected with horseradish peroxidase (HRP)–conjugated antibody (170–6515, 172–1011, 1720–1011, 1:1,000; Bio-Rad), which was visualized by chemiluminescence with Clarity Western ECL substrate (Bio-Rad) and imaged using the LAS-500 Imaging System (General Electric, Boston, MA, USA). The resulting band sizes were resolved using Precision Plus Protein™ Kaleidoscope™ Prestained Protein Standard (1610375, Bio-Rad). For autoantibody detection, the Western blot on RCSC and retina lysates were separated and run on the gel as described above. Following blocking, membranes were incubated with Goat Anti-Mouse IgG (Heavy + Light)-HRP conjugate (170–6516, 1:1,000; Bio-Rad) overnight and following PBS-T washing detected using the LAS-500 Imaging System (General Electric). After the detection of autoantibodies, the membranes were incubated with β-actin (PA1–21167; 1:2,000; Thermo Fisher Scientific, Waltham, MA, USA) for the confirmation of equal loading. Resulting bands of WB targets and IgG were quantified using Image J in the positive digital photographs of the membranes per formula: Relative abundance (RA)=(Target band intensity)/(β-actin intensity). Samples from 4 separate mice per group were used in quantification of the WB targets and samples from 3 mice per group for IgG quantification. Representative WB images are presented in the figures.

Primary RPE cell cultures and treatments and immunostaining

RPE cells were isolated from adult (six-month-old) C57BL6-WT mice by careful dissection of the eye globe on ice and removal of the anterior chamber and retina. The eyecup was then incubated with trypsin Gibco™ Trypsin-ethylenediamine tetra-acetic acid (0.25%) for 40 min with the RPE cell layer facing down. Following the initial digestion, the RPE cells were released by gentle shaking of the eyecup with sterile forceps. The isolated RPE cells were cultured with an N1 complete medium on attachment factor (4Z0–201; Cell systems)-coated slides Millicell EZ slides (Millipore, Billerica, MA, USA) according to the protocol described elsewhere (Fernandez-Godino et al., 2016) for 4 weeks. The cells were mildly fixed in HistoChoice Molecular Biology fixative (H120–4L, VWR Life Science, Radnor, PA, USA)Life Science) for 10 minutes, permeabilized by incubation in 0.05% Triton X-100

for 10 minutes, and blocked with 10% normal goat serum for 1 h at room temperature (RT). The samples were then incubated with primary antibodies, CXCL13, and N-cadherin (Table 2). After PBS-T washing, samples were then incubated with goat anti-rabbit Alexa Fluor 488 (A-11034, 1:1000, Thermo-Fisher), and goat anti-mouse Cyanine5 (A10524, 1:1000, Thermo Fisher Scientific, Waltham, MA, USA). The cell nuclei were visualized by incubation with DAPI; (1:5000; Sigma). The slides were mounted with a ProLong Diamond antifade reagent (Thermo Fisher Scientific, Waltham, MA, USA).

Statistical Analysis

All experiments were performed in triplicates. Experimental values were expressed as the mean ± standard deviation (SD) for the respective groups. Statistical analyses were performed with GraphPad Prism software (https://www.graphpad.com/scientific-software/prism/). A two-way ANOVA with Tukey multiple comparisons was used. A p-value of less than 0.05 was considered significant. The following designations for the *P*-value were as follows: n.s. $P > 0.05$; * $P < 0.05$; ** $P < 0.01$; *** $P < 0.001$. Post-hoc power of the study was evaluated using the G*Power 3.1.9.7 software, F tests - ANOVA: Fixed effects, omnibus, one-way with α err prob = 0.05, and the effect size determined from the datasets. The power of the study (1-β err prob) was calculated to be = >0.9 for both in vivo and ex vivo observations.

Supplementary Material

Refer to Web version on PubMed Central for supplementary material.

Acknowledgments

The authors would like to acknowledge the following contributors: Allen Raye (University of Missouri Department of Biomedical Sciences, Columbia, Missouri, USA) and Lijuan Fan (University of Missouri, Columbia, Missouri, USA) for assistance with animal resources; Molecular Cytology core (University of Missouri, Columbia, Missouri, USA) for technical assistance with confocal imaging; Ms. Sharon Morey (University of Missouri, Department of Ophthalmology Columbia, Missouri, USA) for editing the manuscript; Ms. Catherine Brooks J. (University of Missouri, Department of Ophthalmology Columbia, Missouri, USA) for “masked” quantification and additional language corrections.

An early version of this work was deposited to the preprint server Biorxiv.org https://www.biorxiv.org/content/10.1101/868851v1 under the title “Age-related macular degeneration-like phenotypic features develop at the early ages of Cxcr5/Nrf2 double knockout mice: An accelerated AMD model” and was assigned the DOI: 10.1101/868851

Funding

Dr. Hu Huang’s research was supported by NIH grant R01 EY027824 and Missouri University start-up funds.

References

Ambati J, Anand A, Fernandez S, Sakurai E, Lynn BC, Kuziel WA, Rollins BJ, Ambati BK, 2003 An animal model of age-related macular degeneration in senescent Ccl-2- or Ccr-2-deficient mice. Nat Med 9, 1390–1397. [PubMed: 14566334]

Anderson DH, Mullins RF, Hageman GS, Johnson LV, 2002 A role for local inflammation in the formation of drusen in the aging eye. Am J Ophthalmol 134, 411–431. [PubMed: 12208254]

Baba T, Bhutto IA, Merges C, Grebe R, Emmert D, McLeod DS, Armstrong D, Lutty GA, 2010 A rat model for choroidal neovascularization using subretinal lipid hydroperoxide injection. Am J Pathol 176, 3085–3097. [PubMed: 20395434]

Bartolini D, Dallaglio K, Torquato P, Piroddi M, Galli F, 2018 Nrf2-p62 autophagy pathway and its response to oxidative stress in hepatocellular carcinoma. Transl Res 193, 54–71. [PubMed: 29274776]

Bellezza I, 2018 Oxidative Stress in Age-Related Macular Degeneration: Nrf2 as Therapeutic Target. Front Pharmacol 9, 1280. [PubMed: 30455645]

Bhutto I, Lutty G, 2012 Understanding age-related macular degeneration (AMD): relationships between the photoreceptor/retinal pigment epithelium/Bruch's membrane/choriocapillaris complex. Mol Aspects Med 33, 295–317. [PubMed: 22542780]

Biswas S, Sengupta S, Roy Chowdhury S, Jana S, Mandal G, Mandal PK, Saha N, Malhotra V, Gupta A, Kuprash DV, Bhattacharyya A, 2014 CXCL13-CXCR5 co-expression regulates epithelial to mesenchymal transition of breast cancer cells during lymph node metastasis. Breast Cancer Res Treat 143, 265–276. [PubMed: 24337540]

Chang YW, Singh KP, 2019 Nicotine-induced oxidative stress contributes to EMT and stemness during neoplastic transformation through epigenetic modifications in human kidney epithelial cells. Toxicol Appl Pharmacol 374, 65–76. [PubMed: 31047982]

Cho Y, Wang JJ, Chew EY, Ferris FL 3rd, Mitchell P, Chan CC, Tuo J, 2009 Toll-like receptor polymorphisms and age-related macular degeneration: replication in three case-control samples. Invest Ophthalmol Vis Sci 50, 5614–5618. [PubMed: 19628747]

Combadiere C, Feumi C, Raoul W, Keller N, Rodero M, Pezard A, Lavalette S, Houssier M, Jonet L, Picard E, Debre P, Sirinyan M, Deterre P, Ferroukhi T, Cohen SY, Chauvaud D, Jeanny JC, Chemtob S, Behar-Cohen F, Sennlaub F, 2007 CX3CR1-dependent subretinal microglia cell accumulation is associated with cardinal features of age-related macular degeneration. J Clin Invest 117, 2920–2928. [PubMed: 17909628]

Cousins SW, Espinosa-Heidmann DG, Alexandridou A, Sall J, Dubovy S, Csaky K, 2002 The role of aging, high fat diet and blue light exposure in an experimental mouse model for basal laminar deposit formation. Exp Eye Res 75, 543–553. [PubMed: 12457866]

Curcio CA, 2018 Soft Drusen in Age-Related Macular Degeneration: Biology and Targeting Via the Oil Spill Strategies. Invest Ophthalmol Vis Sci 59, AMD160–AMD181. [PubMed: 30357336]

Datta S, Cano M, Ebrahimi K, Wang L, Handa JT, 2017 The impact of oxidative stress and inflammation on RPE degeneration in non-neovascular AMD. Prog Retin Eye Res 60, 201–218. [PubMed: 28336424]

Edwards AO, Chen D, Fridley BL, James KM, Wu Y, Abecasis G, Swaroop A, Othman M, Branham K, Iyengar SK, Sivakumaran TA, Klein R, Klein BE, Tosakulwong N, 2008 Toll-like receptor polymorphisms and age-related macular degeneration. Invest Ophthalmol Vis Sci 49, 1652–1659. [PubMed: 18385087]

Edwards AO, Ritter R 3rd, Abel KJ, Manning A, Panhuysen C, Farrer LA, 2005 Complement factor H polymorphism and age-related macular degeneration. Science 308, 421–424. [PubMed: 15761121]

Fernandez-Godino R, Garland DL, Pierce EA, 2016 Isolation, culture and characterization of primary mouse RPE cells. Nat Protoc 11, 1206–1218. [PubMed: 27281648]

Hageman GS, Luthert PJ, Victor Chong NH, Johnson LV, Anderson DH, Mullins RF, 2001 An integrated hypothesis that considers drusen as biomarkers of immune-mediated processes at the RPE-Bruch's membrane interface in aging and age-related macular degeneration. Prog Retin Eye Res 20, 705–732. [PubMed: 11587915]

Haines JL, Hauser MA, Schmidt S, Scott WK, Olson LM, Gallins P, Spencer KL, Kwan SY, Noureddine M, Gilbert JR, Schnetz-Boutaud N, Agarwal A, Postel EA, Pericak-Vance MA, 2005 Complement factor H variant increases the risk of age-related macular degeneration. Science 308, 419–421. [PubMed: 15761120]

Hollyfield JG, Bonilha VL, Rayborn ME, Yang X, Shadrach KG, Lu L, Ufret RL, Salomon RG, Perez VL, 2008 Oxidative damage-induced inflammation initiates age-related macular degeneration. Nat Med 14, 194–198. [PubMed: 18223656]

Hollyfield JG, Perez VL, Salomon RG, 2010 A hapten generated from an oxidation fragment of docosahexaenoic acid is sufficient to initiate age-related macular degeneration. Mol Neurobiol 41, 290–298. [PubMed: 20221855]

Huang H, Liu Y, Wang L, Li W, 2017 Age-related macular degeneration phenotypes are associated with increased tumor necrosis-alpha and subretinal immune cells in aged Cxcr5 knockout mice. PLoS One 12, e0173716. [PubMed: 28282423]

Iizuka T, Ishii Y, Itoh K, Kiwamoto T, Kimura T, Matsuno Y, Morishima Y, Hegab AE, Homma S, Nomura A, Sakamoto T, Shimura M, Yoshida A, Yamamoto M, Sekizawa K, 2005 Nrf2-deficient mice are highly susceptible to cigarette smoke-induced emphysema. Genes Cells 10, 1113–1125. [PubMed: 16324149]

Imamura Y, Noda S, Hashizume K, Shinoda K, Yamaguchi M, Uchiyama S, Shimizu T, Mizushima Y, Shirasawa T, Tsubota K, 2006 Drusen, choroidal neovascularization, and retinal pigment epithelium dysfunction in SOD1-deficient mice: a model of age-related macular degeneration. Proc Natl Acad Sci U S A 103, 11282–11287. [PubMed: 16844785]

Klaver CC, Kliffen M, van Duijn CM, Hofman A, Cruts M, Grobbee DE, van Broeckhoven C, de Jong PT, 1998 Genetic association of apolipoprotein E with age-related macular degeneration. Am J Hum Genet 63, 200–206. [PubMed: 9634502]

Klein RJ, Zeiss C, Chew EY, Tsai JY, Sackler RS, Haynes C, Henning AK, SanGiovanni JP, Mane SM, Mayne ST, Bracken MB, Ferris FL, Ott J, Barnstable C, Hoh J, 2005 Complement factor H polymorphism in age-related macular degeneration. Science 308, 385–389. [PubMed: 15761122]

Lennikov A, Saddala MS, Mukwaya A, Tang S, Huang H, 2019 Autoimmune-Mediated Retinopathy in CXCR5-Deficient Mice as the Result of Age-Related Macular Degeneration Associated Proteins Accumulation. Front Immunol 10, 1903. [PubMed: 31474986]

Malek G, Johnson LV, Mace BE, Saloupis P, Schmechel DE, Rickman DW, Toth CA, Sullivan PM, Bowes Rickman C, 2005 Apolipoprotein E allele-dependent pathogenesis: a model for age-related retinal degeneration. Proc Natl Acad Sci U S A 102, 11900–11905. [PubMed: 16079201]

Mattapallil MJ, Wawrousek EF, Chan CC, Zhao H, Roychoudhury J, Ferguson TA, Caspi RR, 2012 The Rd8 mutation of the Crb1 gene is present in vendor lines of C57BL/6N mice and embryonic stem cells, and confounds ocular induced mutant phenotypes. Invest Ophthalmol Vis Sci 53, 2921–2927. [PubMed: 22447858]

Rakoczy PE, Zhang D, Robertson T, Barnett NL, Papadimitriou J, Constable IJ, Lai CM, 2002 Progressive age-related changes similar to age-related macular degeneration in a transgenic mouse model. Am J Pathol 161, 1515–1524. [PubMed: 12368224]

Rojo AI, Innamorato NG, Martin-Moreno AM, De Ceballos ML, Yamamoto M, Cuadrado A, 2010 Nrf2 regulates microglial dynamics and neuroinflammation in experimental Parkinson's disease. Glia 58, 588–598. [PubMed: 19908287]

Saint-Geniez M, Kurihara T, Sekiyama E, Maldonado AE, D'Amore PA, 2009 An essential role for RPE-derived soluble VEGF in the maintenance of the choriocapillaris. Proc Natl Acad Sci U S A 106, 18751–18756. [PubMed: 19841260]

Sarks SH, 1980 Council Lecture. Drusen and their relationship to senile macular degeneration. Aust J Ophthalmol 8, 117–130. [PubMed: 6160841]

Schaumberg DA, Rose L, DeAngelis MM, Semba RD, Hageman GS, Chasman DI, 2014 Prospective study of common variants in CX3CR1 and risk of macular degeneration: pooled analysis from 5 long-term studies. JAMA Ophthalmol 132, 84–95. [PubMed: 24287500]

Tuo J, Smith BC, Bojanowski CM, Meleth AD, Gery I, Csaky KG, Chew EY, Chan CC, 2004 The involvement of sequence variation and expression of CX3CR1 in the pathogenesis of age-related macular degeneration. FASEB J 18, 1297–1299. [PubMed: 15208270]

Velilla S, Garcia-Medina JJ, Garcia-Layana A, Dolz-Marco R, Pons-Vazquez S, Pinazo-Duran MD, Gomez-Ulla F, Arevalo JF, Diaz-Llopis M, Gallego-Pinazo R, 2013 Smoking and age-related macular degeneration: review and update. J Ophthalmol 2013, 895147. [PubMed: 24368940]

Zhao Z, Chen Y, Wang J, Sternberg P, Freeman ML, Grossniklaus HE, Cai J, 2011 Age-related retinopathy in NRF2-deficient mice. PLoS One 6, e19456. [PubMed: 21559389]

Highlights

- CXCR5$^{-/-}$ and NRF2$^{-/-}$ mice are known to develop retinal degeneration with age.
- Both strains were cross-bred to create CXCR5$^{-/-}$.NRF2$^{-/-}$ double knockout (DKO) mice.
- DKO mice develop retinal degeneration at early adult age (4–6 months).
- DKO mice have increased microglia marker TMEM119 and accumulation of IgG in RPE and retina.
- DKO mice demonstrate the accumulation of AMD-associated proteins β-amyloid, Apolipoprotein-E, αB-crystallin in sub-RPE.
- DKO mice are healthy and fertile and can be a useful model of retinal degeneration.

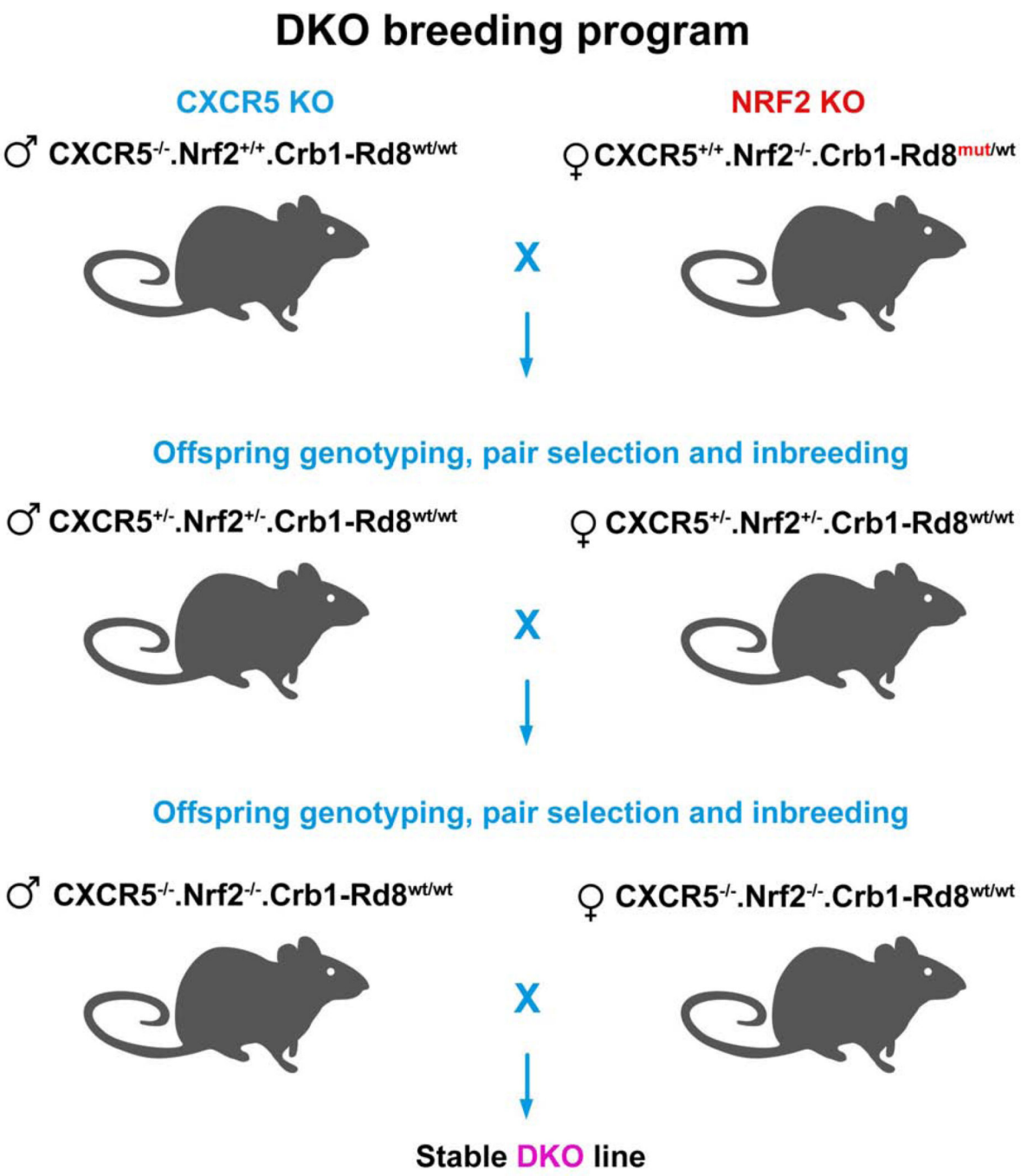

Figure 1.

CXCR5/NRF2 double knockout (DKO) breeding program. The breeding started with the founder mice of male CXCR5 KO ($CXCR5^{-/-}.NRF2^{+/+}.Crb1\text{-}Rd8^{wt/wt}$) and female NRF2 KO ($CXCR5^{+/+}.NRF2^{-/-}.Crb1\text{-}Rd8^{mutant/wt}$). The offspring mice were genotyped. A heterozygous pair of male and female mice with $CXCR5^{+/-}.NRF2^{+/-}.Crb1\text{-}Rd8^{wt/wt}$ were selected and inbred. The second generation of offspring mice was genotyped, breeding pair of mice with DKO genotype $CXCR5^{-/-}.NRF2^{-/-}.Crb1\text{-}Rd8^{wt/wt}$ was selected used propagate the stable DKO mouse line.

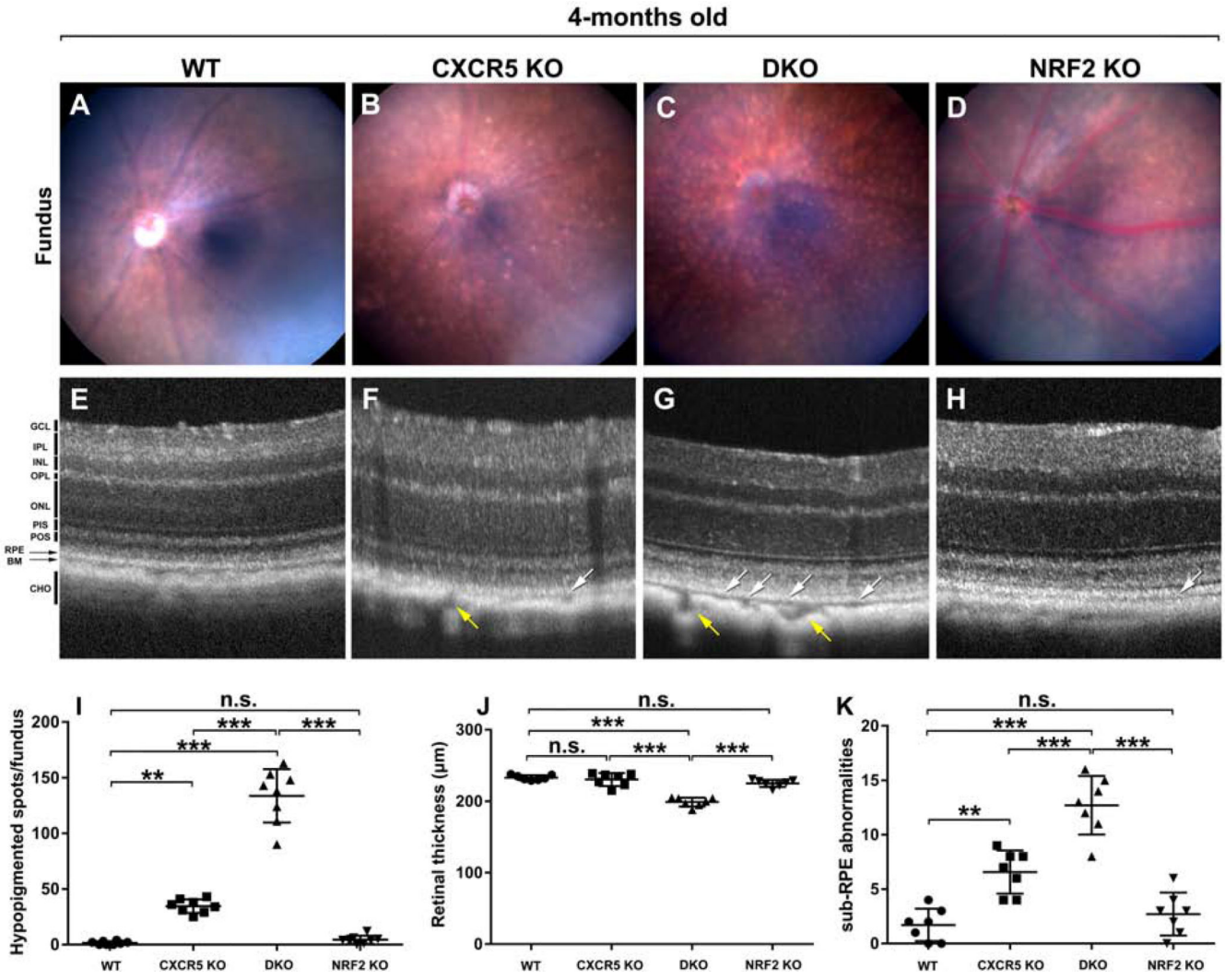

Figure 2.

Fundus and Optical Coherence Tomography evaluations. The representative fundus images C57BL/6 WT (A), CXCR5 KO (B), DKO (C), NRF2 KO (D). The representative OCT images C57BL/6 WT (E), CXCR5 KO (F), DKO (G), and NRF2 KO (H). White arrows indicate sub-RPE abnormalities; yellow arrows indicate enlarged choroidal vessels. The quantification of hypopigmented spots in the fundus images (G), retinal thickness (J), and of sub-RPE abnormalities (K) in the OCT data. The spots numbers on fundus images and the sub-RPE abnormalities were counted by “masked” observer and averaged from images acquired from 8 animals per group (n=8, fundus images); 7 animals per group (n = 7, OCT data). Retinal layers were denoted as follows. GCL - ganglion cell layer. IPL - inner plexiform layer. INL - inner nuclear layer. OPL - outer plexiform layer. ONL - outer nuclear layer. PIS - photoreceptor inner segment. POS - photoreceptor outer segment. RPE - retinal pigment epithelium. BM - Bruch’s membrane. CHO - choroid. *P* values were denoted: n.s. $P > 0.05$; * $P < 0.05$; ** $P < 0.01$; *** $P < 0.001$.

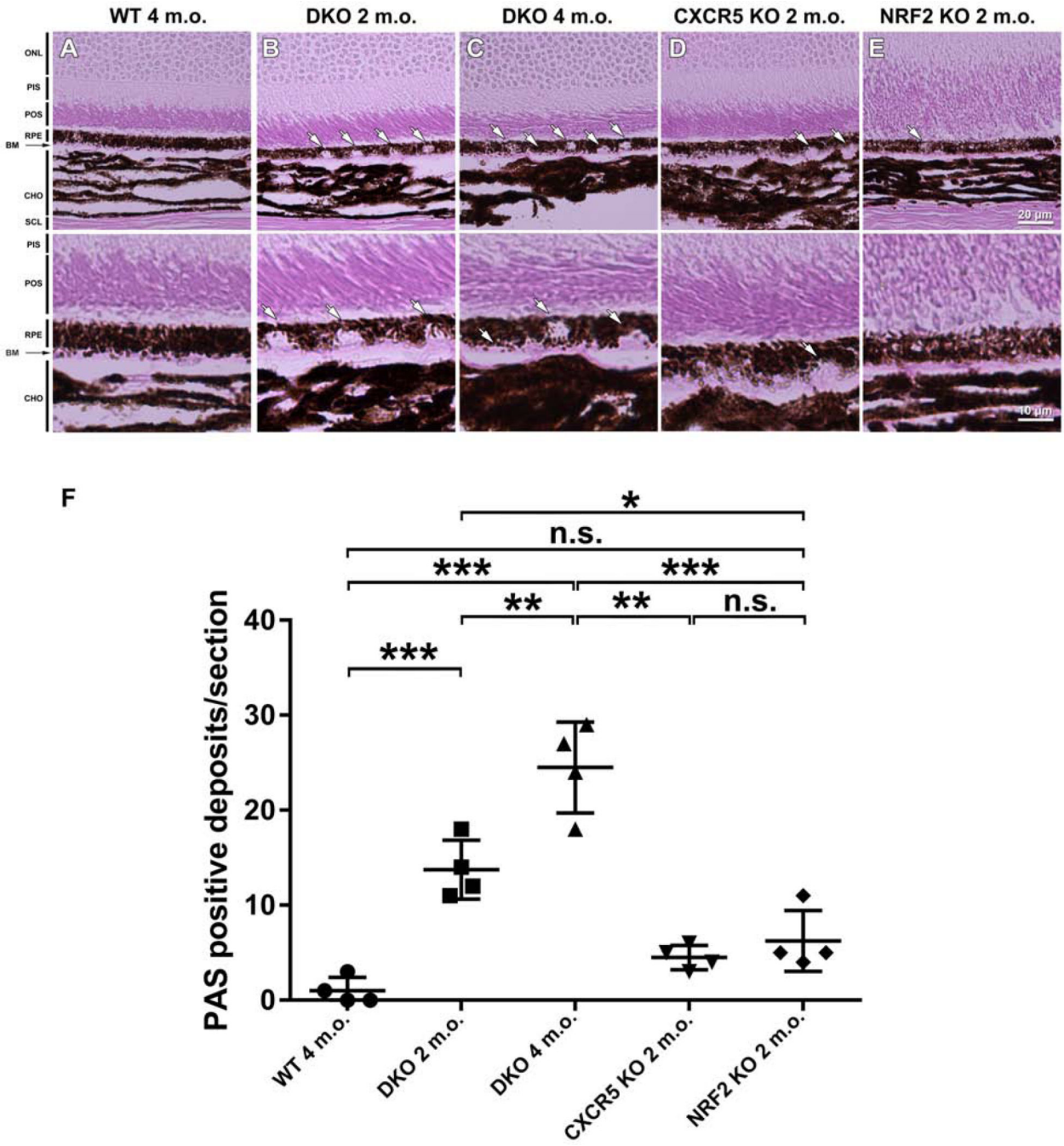

Figure 3.

Increased RPE/sub-RPE deposits in the adult DKO mice, as demonstrated by PAS staining. Four-month-old C57BL/6 WT mice (A), 2- and 4-month-old DKO (B-C), and 4-month-old CXCR5 KO (D) and NRF2 KO (E) mice histological sections were studied, revealing the presence of PAS (+) deposits in RPE-layer of DKO mice at 2-months of age (B); PAS (+) deposits are increasing in size pushing against the thickening Bruch's membrane (visible as a pink layer) into choroid layer in 4-months old DKO mice (C). Retinal layers were denoted as follows: ONL - outer nuclear layer; PIS - photoreceptor inner segment; POS -

photoreceptor outer segment. RPE, retinal pigment epithelium; BM - Bruch's membrane; and CHO - choroid. (F) Quantification of PAS (+) deposits within the RPE and sub-RPE area. The numbers of RPE/sub-RPE deposits were counted and averaged from 4 samples per group (n = 4). *P* values were denoted: n.s. $P > 0.05$; *** $P < 0.001$.

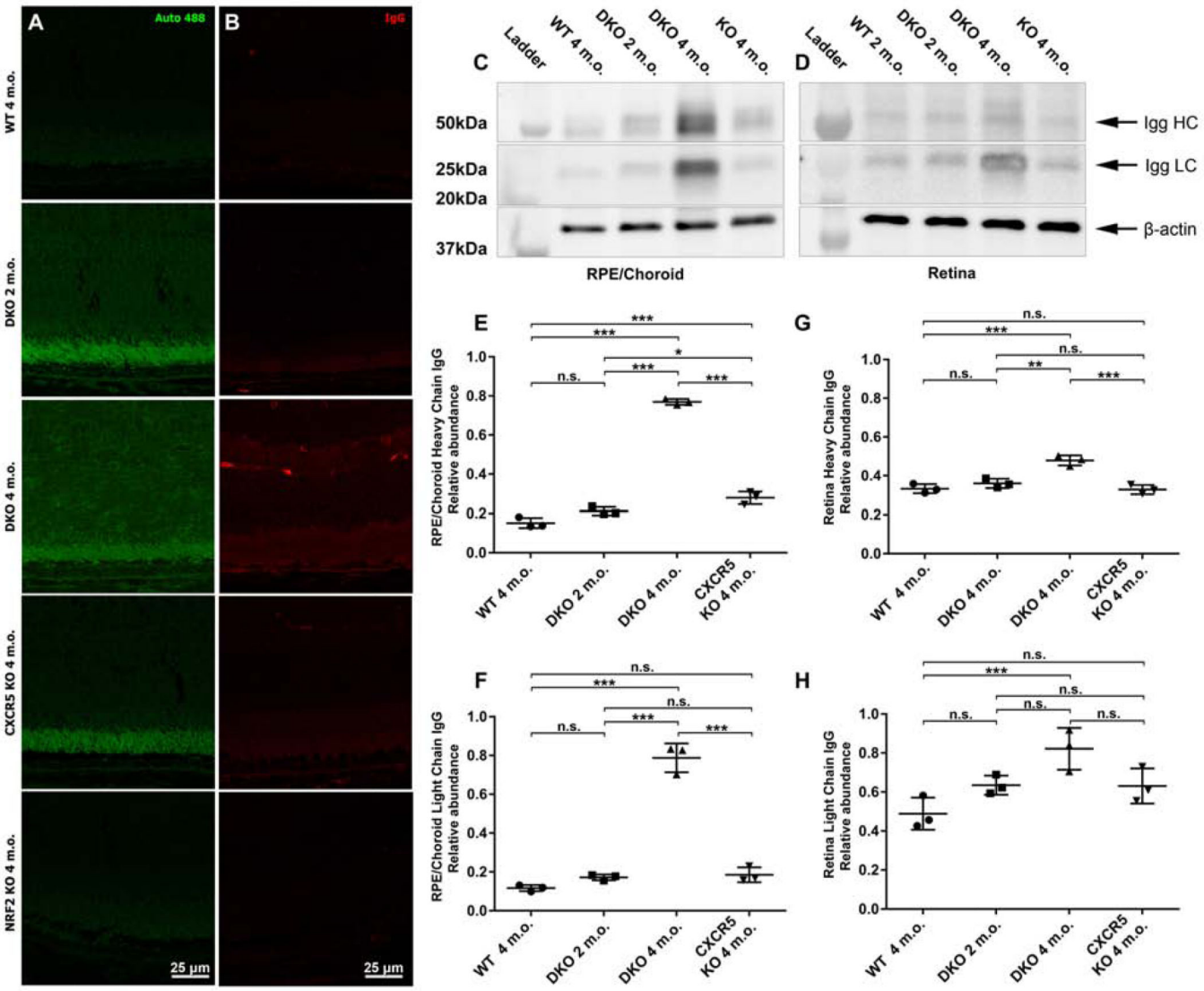

Figure 4.

Increased autofluorescence and IgG depositions at RPE and sub-RPE space of the adult DKO mice. Autofluorescence at 488 nm wavelength (A) and endogenous IgG staining (B) was examined in the retinal sections prepared from WT, DKO 2 and 4 m.o. CXCR5 KO, and NRF2 KO. The representative Western blotting images and quantification results of endogenous IgG heavy (HC) and light chains (LC) from RPE/choroid (C) and the retina (D). The densitometry quantifications for HC and LC in RPE/choroid (E-F) and retina (G-H), were expressed as relative ratios of WB densitometry density between IgG and β-actin (n = 3). *P* values were denoted: n.s. $P > 0.05$; *$P < 0.05$; **$P < 0.01$; ***$P < 0.001$.

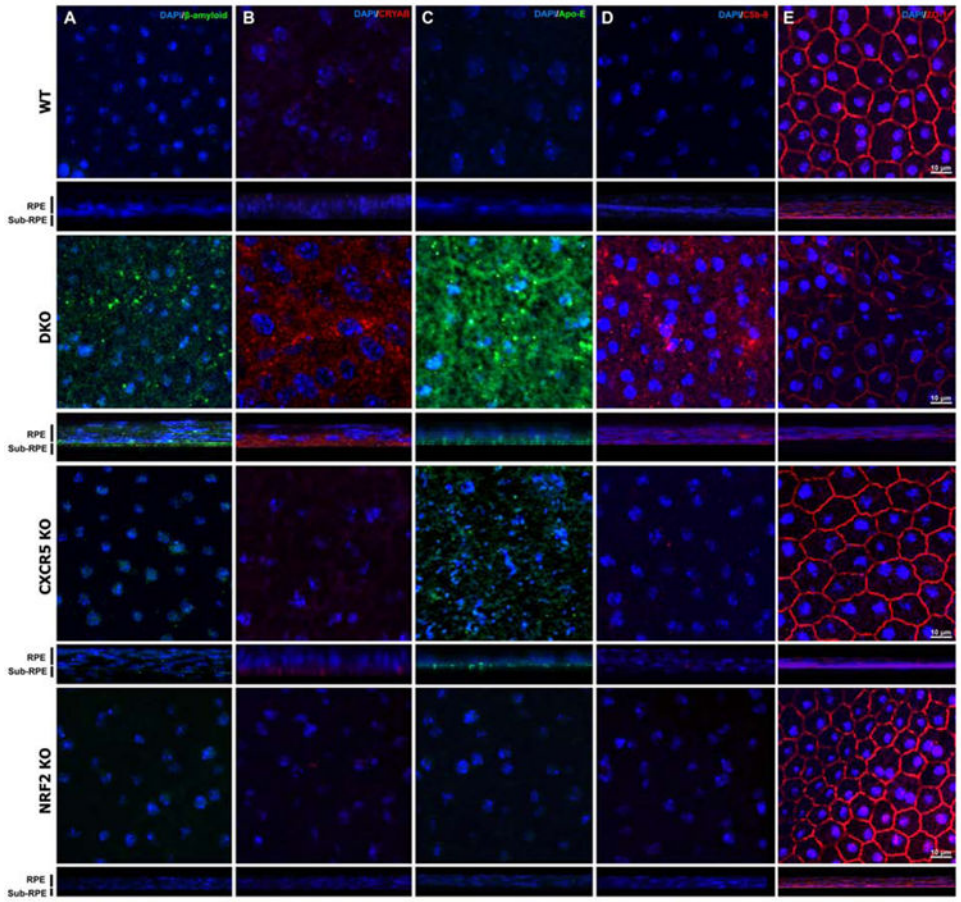

Figure 5.

Increased AMD-associated protein depositions at the sub-RPE spaces of the adult CXCR5$^{-/-}$.NRF2$^{-/-}$ mice. The RPE/Choroid/Scleral complexes flatmounts from 6-month-old from WT, DKO, CXCR5 KO, and NRF2 KO mice were used for immunofluorescence (IF) staining for β-amyloid (A), alpha B-crystallin (CRYAB, B), apolipoprotein E (Apo-E, C), complement 5b-9 (C5b-9, D) and ZO-1 (E). The orthogonal projection of z-stacks demonstrates the sub-RPE location of the signals for β-amyloid, CRYAB, and Apo-E, with complement 5b-9 and ZO-1, detected within the RPE cell layer. Nuclei are counterstained with DAPI.

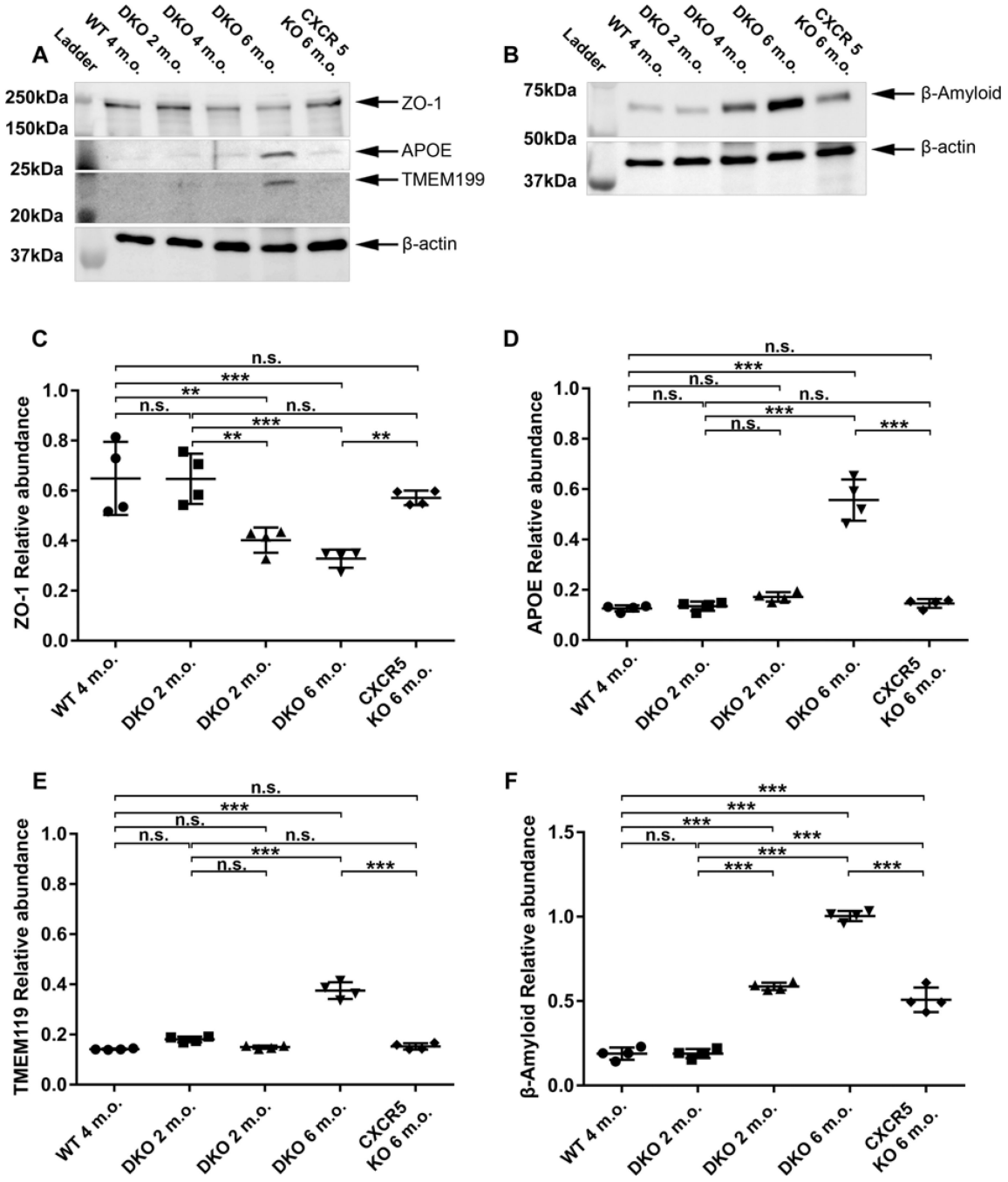

Figure 6.

Reduced zonula occludens-1 (ZO-1) protein levels elevated AMD-associated proteins and microglia marker in the adult DKO. The representative Western blotting images of ZO-1, apolipoprotein E (Apo-E), transmembrane Protein 119 (TMEM119) (A) and β-amyloid (B) in RPE/BM/Choroid protein lysates prepared from WT (6 m.o), DKO (2, 4, 6 m.o.) and CXCR5 KO (6 m.o.) old mice. β-actin used as the loading control. (C-F) The quantification results of the four protein expression levels. The results were expressed as relative ratios of

WB densitometry density between target proteins and β-actin (n = 4). *P* values were denoted: n.s. $P > 0.05$; ** $P < 0.01$; *** $P < 0.001$.

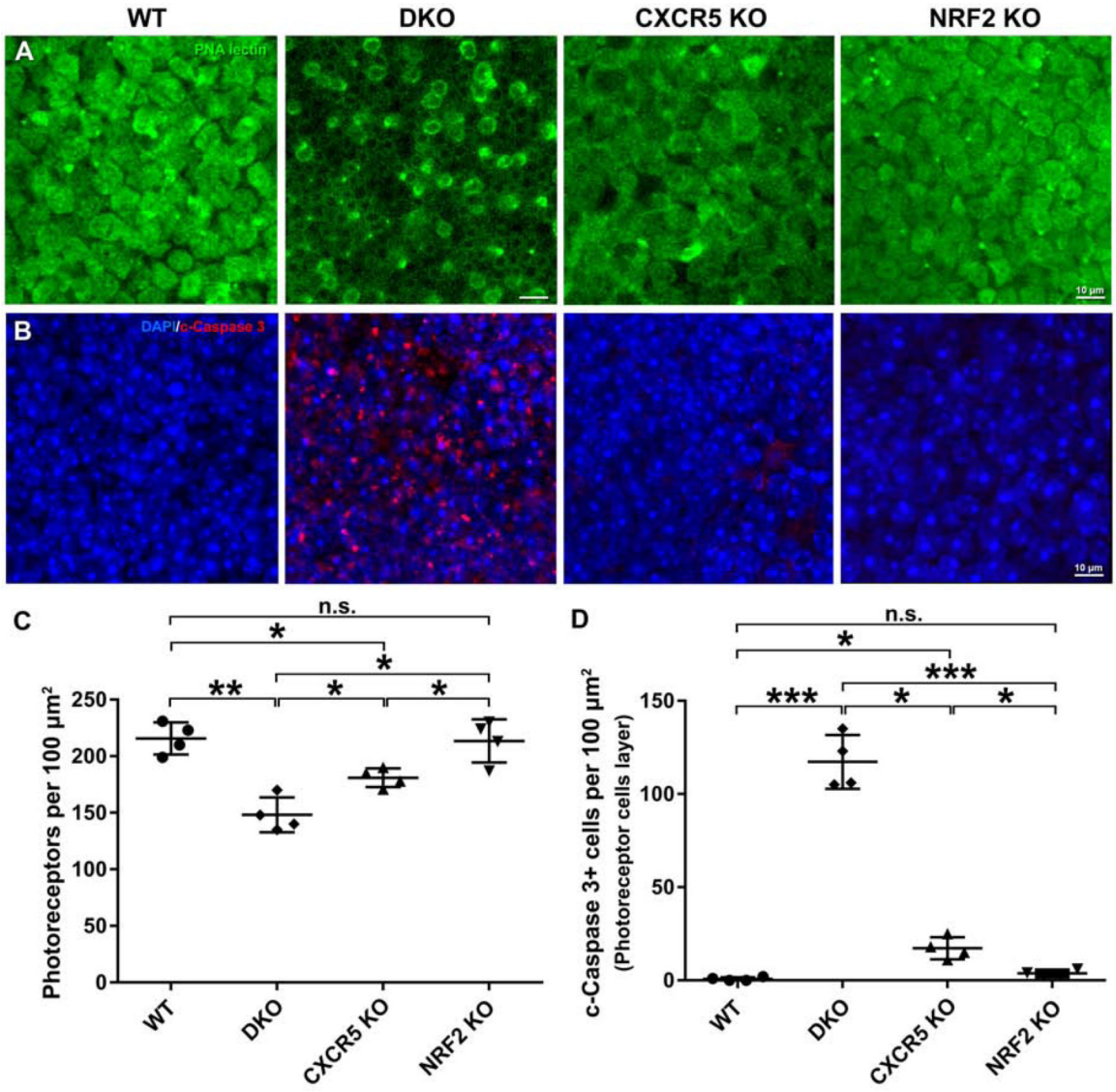

Figure 7.

Increased photoreceptor apoptosis in the adult DKO mice. Retina flatmounts from the 6-month-old WT mice, DKO, CXCR5 KO, and NRF2 KO mice were used for staining and quantification. (A) The staining results of peanut agglutinin (PNA) lectin. (B) The staining results of cleaved (c)-Caspase 3. (C The quantification of PNA(+) photoreceptors. (D) The quantification of the c-Caspase 3 (+) photoreceptors. The values of cell numbers per 100 μm^2 were averaged from 4 retinal samples (n = 4). *P* values were denoted: **P* <0.05; ***P* <0.01; ****P* <0.001.

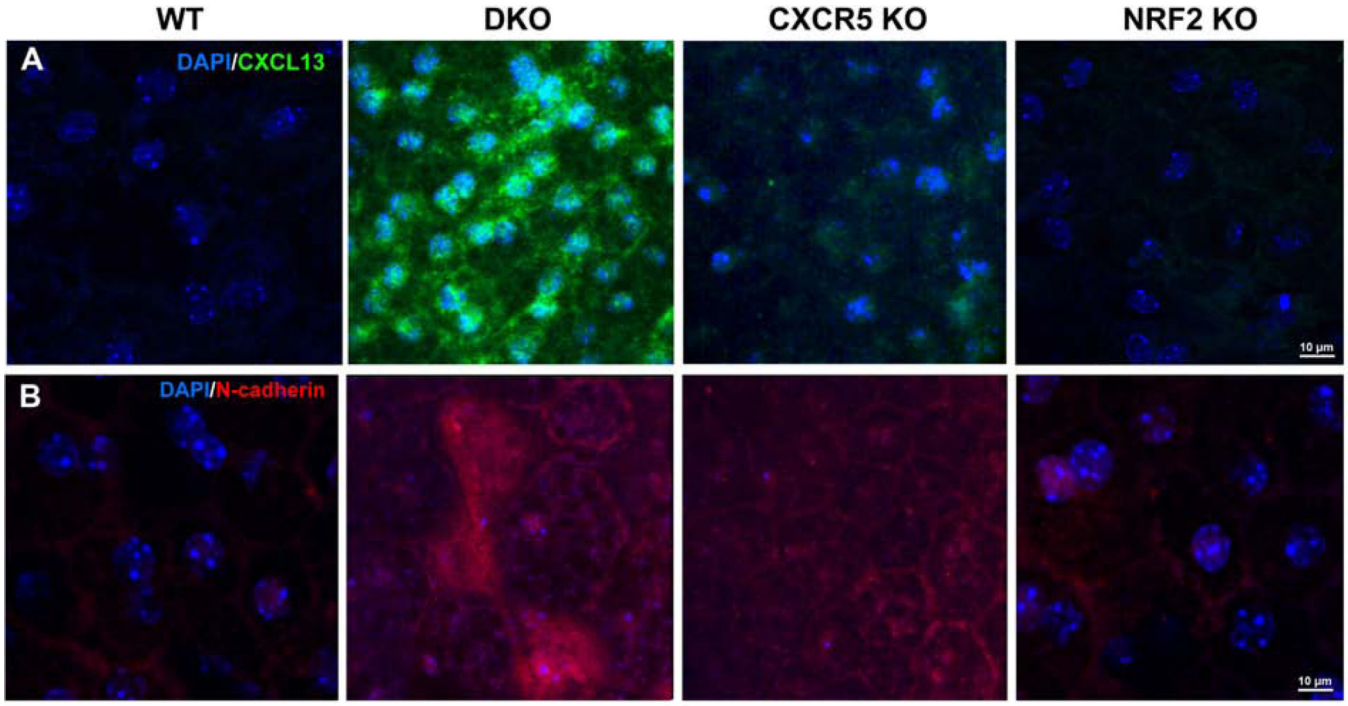

Figure 8.

Increased expression of CXCL13 and N-cadherin in adult DKO mice. Immunofluorescent analysis of CXCL13 (A) and N-cadherin (B) in RCSC complexes flatmounts of 6-month-old WT, DKO, CXCR5 KO, and NRF2 KO mice. Nuclei are counterstained with DAPI.

Table 1:

AMD phenotypic feature in aged CXCR5 KO, aged NRF2 KO, and DKO

	Aged CXCR5$^{-/-}$ (Huang et al., 2017; Lennikov et al., 2019)	**Aged NRF2$^{-/-}$ (Zhao et al., 2011)**	**Adult CXCR5$^{-/-}$.NRF2$^{-/-}$ (Current study)**
Complement pathway	C3d	C3d	C5a-q
Inflammation	TNFa, COX-2 (*in vivo, in vitro*)	IL-6, TNF-α, IL-β (in vitro) (Rojo et al., 2010)	Increased microglial marker (TMEM119)
Oxidative damage	No	Yes	Unknown
Retinal neuron death	Reduced Map2, Lectin (+) photoreceptor loss		Lectin (+) photoreceptor loss, c-Caspase 3(+) increase
Decreased ERG	Yes	Yes	Unknown
Sub-RPE deposits/Drusen	Yes	Yes	Yes
Hypopigmented spots	Yes	Yes	Yes
Increased BM thickness	Yes	Yes	Yes
RPE atrophy	Yes	Yes	Yes
Compromised BRB	Yes	Unknown	Yes
Amyloid accumulation	Yes (β-Amyloid)	Yes (SAP)	Yes (β-Amyloid)
AlphaB-crystallin	Yes	Unknown	Yes
Lipid metabolism	Lipid oil droplet	Lipofuscin accumulation	Apo-E
Immune dysregulation	CD4(+) T cells, Increased IgG	Increased IgG	Increased IgG
Increased autofluorescence	Yes	Yes	Yes
choroidal neovascularization	Yes	Yes	No, enlarged choroidal vessels
Autophagy/lysosomal degradation	Unknown	Yes	Unknown
RPE Vacuole	Yes	Yes	Unknown
CRB1-RD8 mutant	No	No	No

BM – Bruch's membrane; BRB – blood-retinal barrier; ERG – electroretinography; SAP - Serum amyloid P component; RPE – retinal pigment epithelia

Table 2:

List of primary antibodies and dilutions used in the study

Target protein	Produced by	Catalog number	Host	IHC dilution	WB dilution
β-amyloid	Thermo Fisher Scientific, Waltham, MA, USA	36–6900	Rabbit	1:100	1:1000
αB-crystallin	Abcam, Cambridge, MA, USA	Ab151722	Mouse	1:50	1:1000
Apo-E	MilliporeSigma, Burlington, MA, USA	AB947	Goat	1:50	1:1000
Complement 5b-9	MilliporeSigma, Burlington, MA, USA	204903–1MG	Rabbit	1:200	1:1000
cleaved-caspase 3	Cell Signaling Technology, Danvers, MA, USA	D175	Rabbit	1:100	1:1000
ZO-1	Thermo Fisher Scientific, Waltham, MA, USA	61–7300	Rabbit	1:100	1:1000
TMEM119	Thermo Fisher Scientific, Waltham, MA, USA	ab209064	Rabbit	1:100	1:1000
β-actin	Thermo Fisher Scientific, Waltham, MA, USA	MA5–15739	Mouse	1:200	1:2000
CXCL13	Thermo Fisher Scientific, Waltham, MA, USA	PA5–47018	Rabbit	1:100	1:1000
N-cadherin	Thermo Fisher Scientific, Waltham, MA, USA	33–3900	Mouse	1:100	1:1000